Validation of tropospheric ties at the test setup GNSS co-location site Potsdam

Chaiyaporn Kitpracha[1,2], Robert Heinkelmann[2], Markus Ramatschi[2], Kyriakos Balidakis[2], Benjamin Männel[2], and Harald Schuh[1,2]

[1]Technische Universität Berlin, Chair of Satellite Geodesy, Kaiserin-Augusta-Allee 104-106, 10553 Berlin, Germany
[2]GFZ German Research Centre for Geosciences, Space Geodetic Techniques, Telegrafenberg, 14473 Potsdam, Germany

Correspondence: Chaiyaporn Kitpracha (chaiyaporn.kitpracha@gfz-potsdam.de)

Abstract. Atmospheric ties are theoretically affected by the height differences between antennas at the same site and the meteorological conditions. However, there is often a discrepancy between the expected zenith delay differences and those estimated from geodetic analysis, potentially degrading a combined solution employing atmospheric ties. In order to investigate the possible effects on GNSS atmospheric delay, this study set up an experiment of four co-located GNSS stations of the same

5 type, both antenna and receiver. Specific height differences for each antenna w.r.t the reference antenna are given. One antenna was equipped with a radome at the same height and type as a antenna close to the ground. In addition, a meteorological sensor was used for meteorological data recording. The results show that tropospheric ties from the analytical equation based on meteorological data from GPT3, Numerical Weather Model, and in-situ measurements, and ray-traced tropospheric ties, reduced the bias of zenith delay roughly by 72%. However, the in-situ tropospheric ties yield the best precision in this study.

10 These results demonstrate, that the instrument effects on GNSS zenith delays were mitigated by using the same instrument. In contrast, the radome causes unexpected bias of GNSS zenith delays in this study. Additionally, multipath effects at low-elevation observations degraded the tropospheric east gradients.

1 Introduction

15 Nowadays, many weather services assimilate Global Navigation Satellite Systems (GNSS)-derived atmospheric delays and/or atmospheric horizontal gradients into their forecast products (Dousa and Vaclavovic, 2014). Atmospheric water vapour refracts the signals employed by GNSS, an effect that is quantified by the estimation of atmospheric delay coefficients (typically zenith delays and gradients) during the data analysis. The generation of PWV with GNSS only requires knowledge about the in-situ atmospheric pressure (c.f. Nilsson et al. (2013)) because the data and models are accurate enough to allow us assume that

20 the Zenith Wet Delays (ZWD) estimate from GNSS data analysis is related to what actually happens aloft a station in terms of water vapor distribution. The determination of atmospheric delays, however, is correlated with other parameters, most of all with the station height and the station clock, and can be affected by external circumstances, such as multipath signal and

antenna-dependent biases. Our work contributes to the assessment of the quality of atmospheric delays from GNSS as an atmospheric measurement technique.

One of the essential products in the field of space geodesy, the International Terrestrial Reference Frame (ITRF) (e.g., Altamimi et al. (2016)), is utilized as a reference for monitoring changes in the Earth system. An accuracy and stability of 1 mm and 0.1 mm/year, respectively, of the reference frame have to be met as required by the global geodetic observing system (GGOS) (Plag et al., 2009; Männel et al., 2019) to measure effects such as sea-level rise, or tectonic plate motion. The ITRF is currently being obtained from a combination of space geodetic techniques based on station coordinates (local ties) and Earth Orientation Parameters (EOP) (global ties). However, the accuracy and stability of the latest ITRF2014 still do not reach the GGOS requisites. Since the signals employed by co-located space geodetic techniques (e.g., VLBI, GNSS, DORIS, and SLR) are delayed owing to the same overlying atmosphere, estimates of that delay (zenith delays and gradients) could also be utilized to tie the techniques together, in addition to local ties and global ties. A strong correlation exists between atmospheric parameters, especially zenith tropospheric delay (ZTD), and the height component (Schuh and Böhm, 2013). Therefore, an improvement in the ZTD estimation can theoretically improve the co-located station positions (Pollet et al., 2014). Thus, the atmospheric parameters at the same observing site (atmospheric ties) could improve the combination of space geodetic techniques to establish an ITRF meeting the GGOS goals. Typically, the quality of the ITRF depends on the accuracy of ties, which are used to link space geodetic techniques (Ray and Altamimi, 2005). To reach the target of GGOS, local ties with a millimeter accuracy or even better are required (Glaser et al., 2019) and atmospheric ties should be determined with millimeter accuracy as well. The main threats and error sources for local ties are discontinuities in time series due to instrumental change, environmental effects, and local obstructions (Pinzón and Rothacher, 2018). Similar causes might exist for atmospheric ties as well.

Many studies compare ZTD parameters at co-location sites from space geodetic techniques with numerical weather models. In general, these parameters have an excellent agreement of better than 1 cm in RMS and are consistent with numerical weather models and other meteorological measurements (Pollet et al., 2014). Teke et al. (2013) showed ZTD and gradients during CONT02 to CONT11 derived from observations of GNSS, VLBI, DORIS, water vapor radiometers (WVR), and numerical weather model. They found that the best agreement between VLBI and GNSS was roughly 5 to 6 mm at most co-location sites for CONT02, CONT05, CONT08, and CONT11 campaigns. Additionally, they stated that the agreement and the accuracy of the troposphere parameters mainly depend on the humidity in the atmosphere. Pollet et al. (2014) also found that the consistency of ZTD parameters depends on the humidity level and the number of observations per estimated ZTD parameter. Heinkelmann et al. (2016) compared the atmospheric parameters derived by DORIS, GPS, VLBI, and numerical weather models at five co-located sites during CONT14. Moreover, they assessed ray-traced atmospheric parameters at different reference points at co-location sites. They found out that the different reference positions cause a significant difference in zenith total delay, whereas the differences of gradients are not so significant. They found that special weather events could introduce a large discrepancy in atmospheric parameters between space geodetic techniques. Also, DORIS determined less precise atmospheric parameters due to the poor observation geometry. Kitpracha et al. (2020) analyzed time series of the differences of tropospheric delays at the Wettzell co-location site using three different GNSS observations (e.g., L1, L2, and the ionosphere-free linear combination

of dual-frequency (L3)) to estimate troposphere delays. They found that the instrumental changes cause significant jumps in the time series of the tropospheric parameter differences.

To further investigate the potential instrumental effects on GNSS atmospheric delays in this study, we designed a GNSS co-location site experiment. With this experiment, we expected to learn what are the potential effects of GNSS atmospheric delays. Moreover, we used this experiment to assess the quality of the tropospheric ties for each derivation method and the potential of applying tropospheric ties with sub-daily resolution. In Sect. 2, we describe the GNSS co-location experiment. In Sect. 3, the GNSS data processing is outlined together with the derivation of atmospheric ties from the analytical equation and ray-tracing through a Numerical Weather Model (NWM). In Sect. 4, we discuss the comparison results of ZTD and troposphere north and east gradients from the experiment. In Sect. 5, we summarize the results from the experiment.

2   GNSS co-location experiment

We designed the GNSS co-location experiment to assess whether the expected atmospheric delay differences that are calculated employing either in-situ meteorological observations or weather data match those estimated from the independent geodetic analysis of data collected at these co-located stations. At any site, we expect decreasing zenith delays from nodes of the same observing system with increasing height, at any given time. In order to prove this statement, we set up the experiment on the rooftop of the A20 building at Telegrafenberg, the campus of GFZ, Potsdam, Germany. This experiment used four Septentrio choke-ring antennas (SEPCHOKE B3E6) and Septentrio PolaRx5 receivers. Figure 1 shows the set-up of the experiment. We put the antenna A201 at the highest place. A202 and A203 were placed lower than A201 with two meters and four meters height differences, respectively. Antenna A204 was placed on the same level as A203 but installed with radome (SPKE). Due to the fact that the radome induces some additional signal propagation delay on GNSS observations owing to its material and shape (Schmid, 2009), we expected it to increasing the atmospheric zenith delays differences. The meteorological sensor (Vaisala WXT530) was installed to record air pressure, temperature, and relative humidity; the logging interval was set to every 300 seconds. The precision of meteorological data can be found in Appendix A. The horizontal separation is less than 15 m in this experiment, assuring that all GNSS antennas and the meteorological sensor were subjected to the same atmosphere condition. This experiment was conducted from 30th January to 7th March 2020. Additionally, we used this experiment to assess whether there is any utility in applying tropospheric ties in sub-daily resolution (every hour in this study) with the analytical equation, NWM, and in-situ measurements for GNSS intra-technique combination.

3   Data analysis

3.1   Tropospheric ties

A difference in troposphere delays between GNSS antennas is expected due to the different antenna reference point locations in this experiment, especially due to the height differences. These can be called "tropospheric ties" (Teke et al., 2011; Heinkelmann et al., 2016). We determined tropospheric ties at the GNSS tropospheric delay estimation epochs with various methods
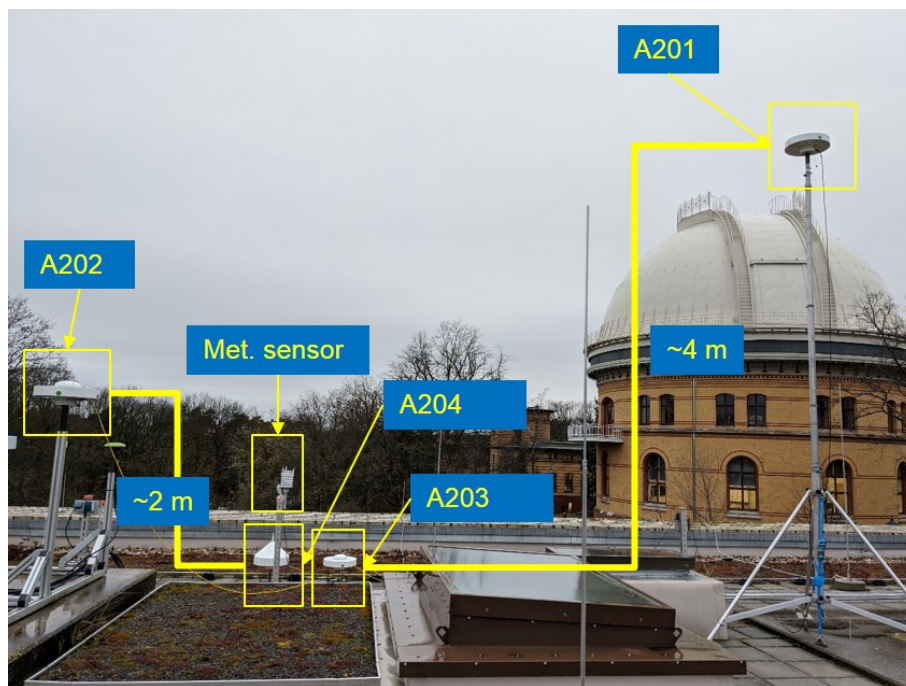
Figure 1. The GNSS co-location experiment set-up on the rooftop of A20 building (Telegrafenberg, Potsdam Germany). The antenna names, height differences, and meteorological sensor are annotated.

and meteorological information and examined their performance. In this study, we defined tropospheric ties using an analytical

90   equation from Teke et al. (2011) based on the height differences and three different meteorological datasets from the Global Pressure Temperature model 3 (GPT3) (Landskron and Böhm, 2018) (T1), ERA5 NWM (T2), and the local meteorological sensor (T3). We used the daily estimated coordinates as input for the analytical equation. The mean coordinates averaged over the entire campaign were used for extracting meteorological parameters from NWM. The meteorological data from the sensor were collected every 300 seconds and linearly interpolated to the estimation epoch. The pressure bias related to the height

95   differences between the meteorological sensor and the GNSS reference point needs to be addressed. Thus, we corrected the pressure data from the meteorological sensor to each GNSS antenna reference point using an analytical equation from Teke et al. (2011). Moreover, tropospheric ties were determined from ERA5 NWM utilizing the ray-tracing algorithm presented by Balidakis et al. (2018) (T4). The effect of horizontal distance was not investigated in this study because the expected gradient differences are well below the capability of the modern GNSS system, as described in Sec. 2.

100   Since the heights are an essential information in tropospheric ties derivation and ray-tracing, we investigated their precision in this study. The variation of the heights of the four antennas for the entire experiment was within 1 cm as presented in Fig. 2. The standard deviation of the height differences was roughly 2 mm. This variation was expected because of many reasons, such as the building has some physical motion due to thermal expansion, satellites orbit and clock errors, and satellites geometry during the day. However, this variation could not affect the derivation of tropospheric ties significantly because tropospheric
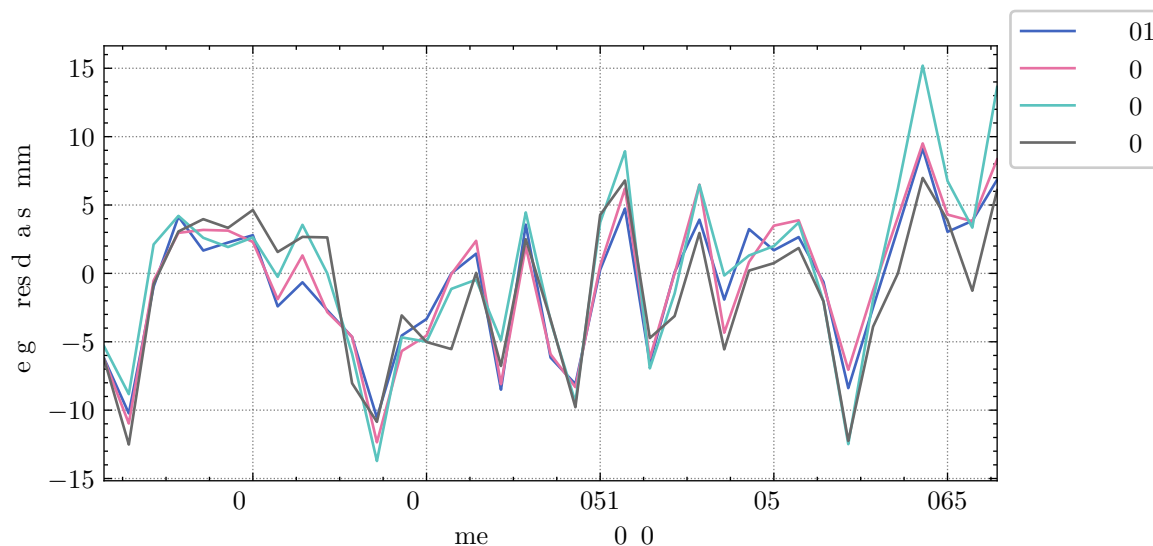
Figure 2. Residual height time series w.r.t mean values for four antennas in the experiment.

105   delay differences at the level of 1 mm require the height differences at the level of 4 m due to the hydrostatic part (Bock et al., 2010).

    Table 1 shows the height differences and mean tropospheric ties between the GNSS antennas from individual methods in this experiment. Tropospheric ties agree very well between individual methods. This is in line with the previous study from Krügel et al. (2007). Additionally, the tropospheric ties magnitude increases with increasing height differences. Figure

110   3 shows the hourly tropospheric ties between A201 and A203 stations during the experiment. The tropospheric ties based on the meteorological sensor, NWM, and ray-tracing show similar variability; however, tropospheric ties based on GPT3 show almost no variation, which is expected given that GPT3 features only annual and semi-annual waves and the duration of the experiment was two weeks only. This shows that all tropospheric ties derivation methods account for the sub-daily atmosphere variation except T1, which contains only annual and semi-annual variations.

115 **3.2   GNSS processing**

In this study, we analyzed GNSS observations using the GFZ software package EPOS.P8 (Uhlemann et al., 2015). Precise Point Positioning (PPP) approach was used based on GFZ final orbit and clocks information (Männel et al., 2020). The GNSS processing includes the estimation of daily station coordinates, hourly zenith tropospheric delays, also hourly horizontal gradients. The orbits are given in the IGS14 reference frame (Rebischung and Schmid, 2016), which is a realization of the ITRF2014,

120   and are consistent with the IERS Conventions 2010 (Petit and Luzum, 2010). The observation sampling rate was five minutes. Dual-frequency GPS and GLONASS code and carrier phase observations were used to perform ionosphere-free combination to eliminate ionospheric effects. The receiver clock parameters were estimated per observation epoch. The a priori zenith total

Table 1. Estimated height differences and mean tropospheric ties from individual methods, referring to the reference point of the individual GNSS reference antenna.

Station pair		Height difference (m)	Mean zenith delay difference (mm)			
Ref.	Rov.		GPT3 (T1)	NWM (T2)	Met. Sensor (T3)	Ray-traced (T4)
A203	A204	-0.010	0.003	0.000	0.003	0.003
A202	A204	1.559	-0.480	-0.481	-0.480	-0.485
A202	A203	1.569	-0.483	-0.483	-0.484	-0.487
A201	A202	2.489	-0.766	-0.768	-0.767	-0.774
A201	A204	4.048	-1.246	-1.250	-1.248	-1.259
A201	A203	4.058	-1.249	-1.252	-1.251	-1.262
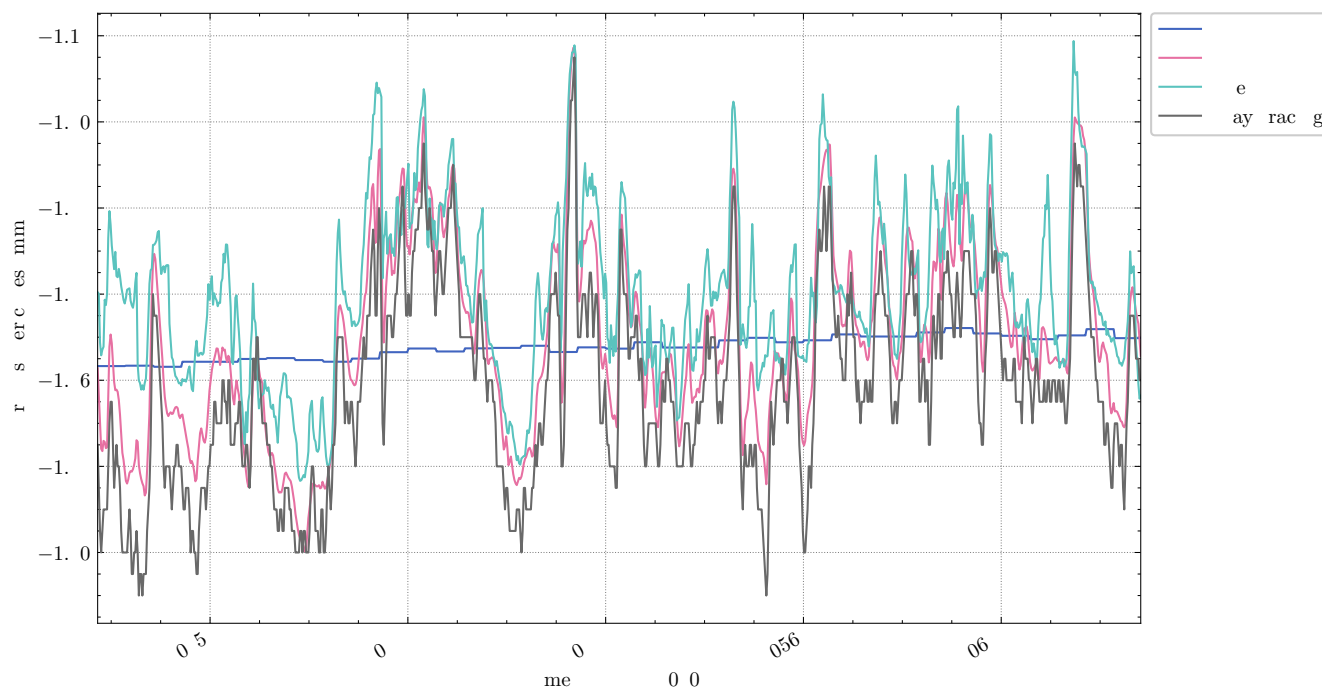
Figure 3. Zenith delay differences during the experiment between A201 and A203 stations from individual methods.

Table 2. Description of ZTD comparison cases

Case	Tropospheric ties method	Meteorological data
S0	not applying ties	x
S1	analytical equation	GPT3
S2	analytical equation	NWM
S3	analytical equation	Meteorological sensor
S4	ray-tracing	NWM

delays (ZTD) were calculated using meteorological information from the Global Pressure Temperature model 2 (GPT2) (La-gler et al., 2013). The Vienna Mapping Function 1 (VMF1) (Böhm et al., 2006) was used to map the slant delays to zenith
125 delays. Chen and Herring (1997) model was used as gradient mapping function. A cut-off elevation angle of seven degrees was applied as well as elevation-dependent observations weighting $1/cos^2 z$ where z is zenith angle.

3.3 Data comparison

We determined six comparison cases between the GNSS stations in the experiment, as presented in Tab. 1. We calculated the mean biases of the differences between time series and the weighted root-mean-square (WRMS) errors. Regarding the
130 ZTD comparison, we calculated five types of ZTD differences, following Table 2. Firstly, we calculated the ZTD differences without applying tropospheric ties (S0). Secondly, we applied tropospheric ties using the analytical equation (Teke et al., 2011) based on meteorological information from GPT3 (S1), NWM (S2), meteorological sensor (S3), and ray-tracing (S4), respectively, before calculating the ZTD differences, in order to assess the performance of tropospheric ties from the individual methods. We performed error propagation from input parameters to calculate the uncertainty of tropospheric ties for each
135 method. The uncertainties of meteorological parameters from GPT3, NWM, and the meteorological sensor can be found in Appendix A. We compared the tropospheric gradients as well and calculated the time series of the differences between estimated gradients for each comparison case. Then, weighted mean biases, weighted standard deviation, and WRMS were calculated for each comparison case. As the GNSS antennas in this experiment observed the same tilt of the atmosphere, we expected no differences in the estimated gradients. Thus, we compared the estimated gradients directly without applying
140 corrections.

According to Fig. 6, the observation geometry is similar for all antennas of the experiment. Therefore, the effects from observation geometry can be neglected in this study.

4   Results

4.1   ZTD comparison

145 We present the comparison of ZTD for each case described in Tab. 2. A selection of the results is provided in Fig. 4 and Tab. 3, while the complete set of results can be found in the electronic supplement.

Figure 4 shows the ZTD differences between A201 and A203 for all cases during the experiment. The bias between A201 and A203 for S0 is -1.70 mm with an empirical standard deviations of 1.60 mm. Meanwhile, the biases for S1, S2, S3, and S4 are -0.48, -0.48, -0.50, and -0.46 mm with a similar empirical standard deviation of S0 for all cases. This result shows that

150 significant biases are mainly caused by the height differences and meteorological conditions. Moreover, tropospheric ties from all methods can significantly mitigate the biases. However, there is no improvement in the empirical standard deviation of the ZTD differences when applying tropospheric ties since the variation of tropospheric ties is less than 0.1 mm, as demonstrated in Fig. 3. This agrees with the previous study by Heinkelmann et al. (2016). According to Tab. 3, this situation applied to the comparison between A201 and A202, A202 and A203 as well. In contrast, we found unexpected biases in the S0 case between

155 A201 and A204. The bias is smaller than expected (less than 0.1 mm) despite the height difference is roughly four meters. Thus, applying tropospheric ties increases the ZTD difference biases, as shown in S1, S2, S3, and S4. These unexpected biases can be seen when comparing A202 and A204, and A203 and A204 as well. They are related to the radome which causes unknown effects in the GNSS ZTD parameters. Therefore, installing a radome should be avoided unless necessary, as recommended in the IGS site guidelines (IGS, 2019).

160 Additionally, we calculated formal errors of tropospheric ties for the particular method in the experiment. The formal errors of T1, T2, T3, and T4 are 34.8, 3.2, 1.6, and 14.1 mm, respectively. T3 yields the best precision in this study because the meteorological sensor provides high precision of the meteorological parameters as presented in Appendix A.

Table 3. Mean biases, standard deviation, and WRMS of the ZTD differences during the experiment for all cases. All values are in millimeters. The results are presented in weighted mean±weighted std. (weighted rms) format.

Station-pair	S0	S1	S2	S3	S4
A201-A202	-1.06±0.98(1.44)	-0.28±1.00(1.03)	-0.28±0.99(1.03)	-0.29±0.99(1.03)	-0.27±0.99(1.03)
A201-A203	-1.70±1.60(2.30)	-0.48±1.63(1.70)	-0.48±1.61(1.68)	-0.50±1.59(1.67)	-0.46±1.63(1.69)
A201-A204	-0.09±1.72(1.73)	1.21±1.80(2.17)	1.20±1.78(2.15)	1.17±1.76(2.11)	1.22±1.80(2.17)
A202-A203	-0.69±1.49(1.64)	-0.20±1.53(1.55)	-0.20±1.52(1.54)	-0.21±1.51(1.52)	-0.19±1.53(1.54)
A202-A204	0.97±1.75(2.00)	1.49±1.80(2.34)	1.48±1.79(2.32)	1.46±1.78(2.30)	1.49±1.80(2.34)
A203-A204	1.66±1.82(2.46)	1.68±1.90(2.54)	1.68±1.88(2.52)	1.67±1.86(2.50)	1.68±1.90(2.54)
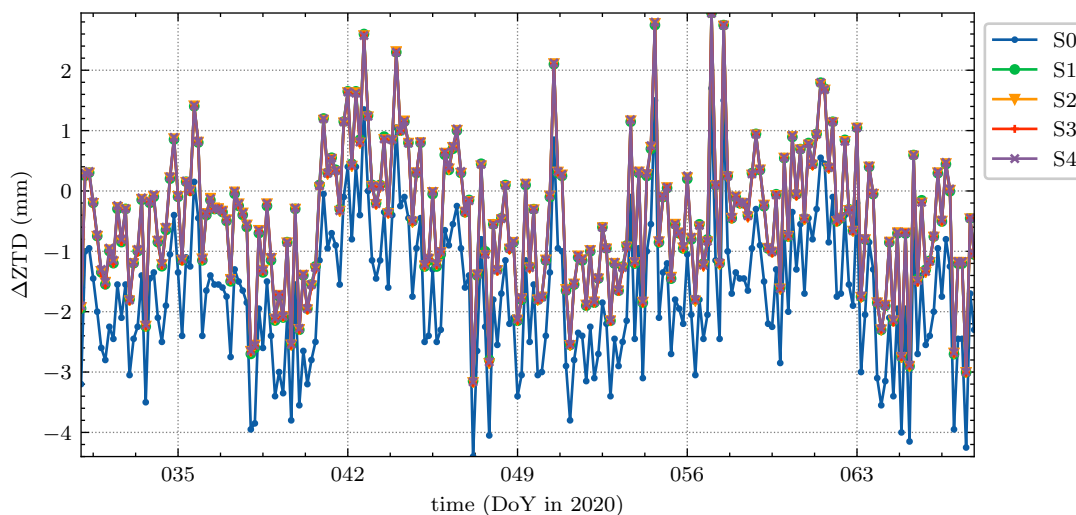
Figure 4. The ZTD differences (smoothed with a four-hours running median filter) between A201 and A203 for all case studies. The height differences is approximately four meters.

4.2 Tropospheric horizontal gradients

In this section, we present the comparison of the tropospheric gradients. For each comparison case, we statistically analyzed
165 both north and east estimated gradients, as mentioned in Sect. 3.3.

Figure 5 shows the comparison of the estimated east gradients between the GNSS antennas during the experiment. The best agreement was found between A201 and A202. The bias and WRMS are approximately 0.1 mm and 0.1 mm, respectively. These are expected because both antennas were installed horizontally close. In contrast, the biases are mostly between 0.1 and 0.2 mm, and the WRMS are at the level of 0.3 mm for the rest of the comparison. These results show that some effects
170 degraded the estimated east gradients in A203 and A204. According to Fig. 1, there were some obstacles around A203 and A204, e.g. shadowing of refractor building, and the antennas were placed close to the ground. Therefore, there is a possibility of larger multipath effects for both antennas. According to Fig. 6, we found large residuals for low-elevation observations in A203 and A204, especially in the east-west direction. This shows that multipath causes effects on the estimated east gradients in A203 and A204 antennas because low-elevation observations are most important for estimating the gradients.

175 Additionally, the biases of the north gradient differences are at the level of 0.1 mm or better for all comparisons according to Tab. 4. The best agreement of the north gradients was found again for A201 and A202. The bias is 0.02 mm and the WRMS is roughly 0.3 mm. Meanwhile, the WRMS for the rest of the differences are approximately 0.4 mm. The north gradient biases were smaller than those of the east gradients in this experiment, except for the small differences between A201 and A202 because the residual north-south observations were smaller than the residual east-west observations as shown in Fig. 6. It is
180 obvious, that the north-south and east-west observations affect north-south and east-west gradients parameters, respectively. However, the WRMS of the differences of the north gradients is higher than that of the east gradients. According to Fig. 6,

there are few observations in the northern part of the skyplot due to the inclination of the GNSS orbits causing a high variation in the estimated north gradient.
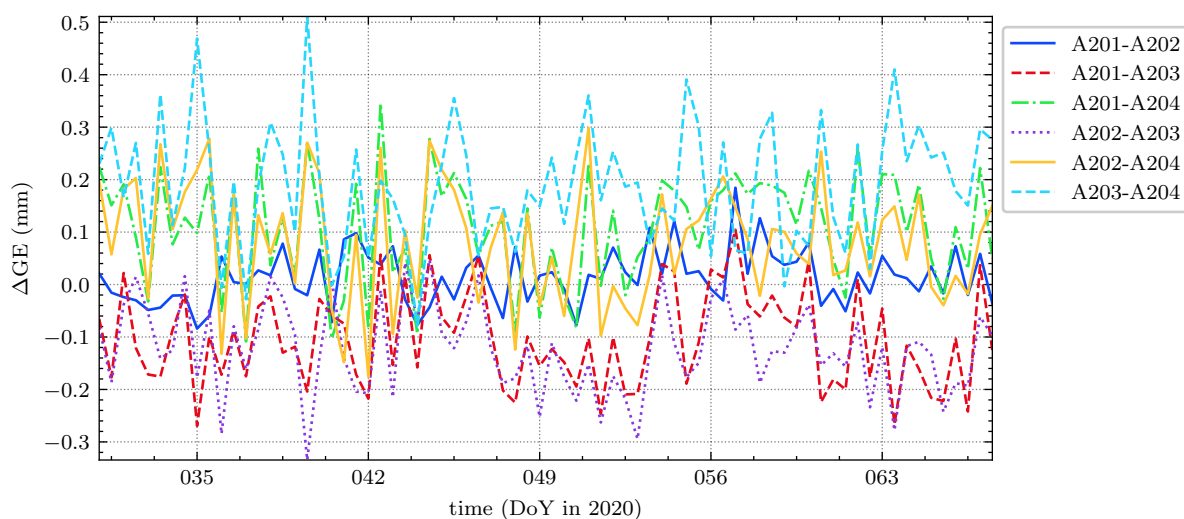
Figure 5. The differences of tropospheric east gradients (smoothed with a 12-hours running median filter) between the GNSS antennas in the experiment.

Table 4. Mean biases and WRMS of the tropospheric gradient differences from the experiment for all comparison cases.

Comparison cases	Differences of mean values (mm)		WRMS (mm)	
	East gradient	North gradient	East gradient	North gradient
A201-A202	0.013	0.027	0.163	0.247
A201-A203	-0.111	0.044	0.321	0.457
A201-A204	0.106	0.101	0.347	0.435
A202-A203	-0.123	0.018	0.314	0.436
A202-A204	0.093	0.073	0.340	0.446
A203-A204	0.215	0.060	0.413	0.447

5 Conclusions

185 This paper investigates the systematic effects in GNSS atmospheric delays and tropospheric ties performance by setting up a GNSS co-location site experiment. According to the results, the application of tropospheric ties on ZTD leads to a reduction

(a) Residual plot of A201 antenna.

(b) Residual plot of A202 antenna.

(c) Residual plot of A203 antenna.

(d) Residual plot of A204 antenna.
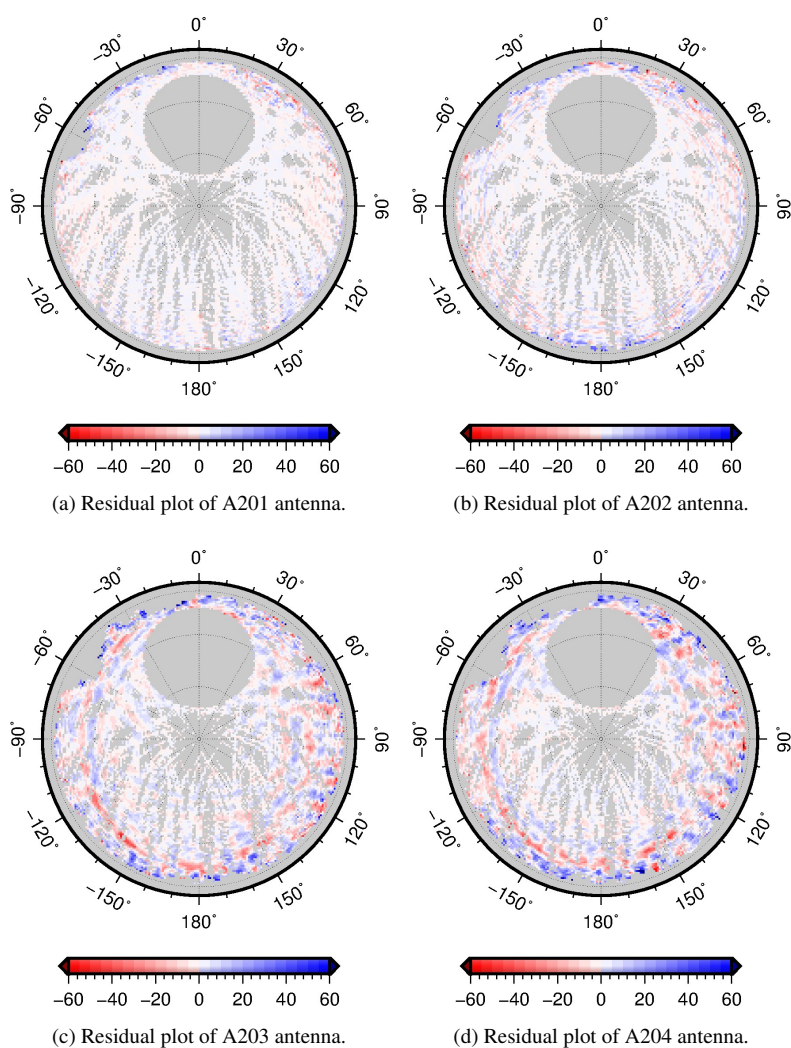
Figure 6. Residuals of ionosphere-free phase observations of A201, A202, A203, and A204 for the entire experiment. All units are in millimeters.

of the mean differences between the antennas by 72 %, i.e., from -1.7 mm to -0.48 mm while the standard deviations remain unaffected for small height differences. These results confirm that the ZTD bias between antennas depends only on the height differences and the meteorological conditions if using the same instrument in a co-location site. Moreover, applying high-

190 frequency tropospheric ties shows insignificant effects for small height differences, as presented in this study. Nevertheless, the radome causes an additional delay on the GNSS measurements. Installing radome should be avoided as recommend by the IGS site guidelines (IGS, 2019). Additionally, tropospheric ties from analytical equations with meteorological data from the standard model, Numerical Weather Model, or in-situ measurements and ray-traced tropospheric ties show similar performance for small height differences between GNSS antennas. However, tropospheric ties from the analytical equation based on in-situ

195 measurement show the best precision in this study. Therefore, a meteorological sensor is recommended to install along with the GNSS station at each co-location site. However, if a meteorological sensor is not available, a Numerical Weather Model can be another option in tropospheric ties determination.

The best agreement of tropospheric gradients was found between A201 and A202, which was expected. However, the multipath effects on low-elevation observations degrade the tropospheric gradients from GNSS, primarily east gradients in this

200 study. Therefore, the GNSS antenna should not be installed close to the ground or an obstacle that causes multipath signals, as recommended by the IGS site guidelines (IGS, 2019). Moreover, lacking observations in the northern part of the sky caused high variation in the north gradients in this experiment.

The technique-dependent systematic effects, such as radome and multipath effects, are the primary sources of biases in the GNSS atmospheric delays and gradients. This statement agrees with the previous study from Steigenberger et al. (2013)

205 that showed multipath effects and radome caused biases in the coordinate estimates that simultaneously affect atmospheric parameters. Therefore, these effects needed to be accounted for, especially multipath effects, to determine precise atmospheric delays from GNSS, necessary for Precipitate Water Vapor determination for climate studies.

Further investigation is required as this experiment was conducted only for a short period of about five weeks. Some potential effects could occur in long-term atmospheric delays, such as severe weather events. Moreover, increasing the distances (both

210 horizontal and vertical) between the GNSS antennas could determine the limitation of the application of tropospheric ties in the combination of atmospheric parameters.

Appendix A: The uncertainties of meteorological parameters

The uncertainties of meteorological parameters, such as pressure, temperature, relative humidity, provided by GPT3, the meteorological sensor, and the Numerical Weather Model, are described in Tab. A1. Unfortunately, the meteorological sensor can

215 not provide water vapor pressure data directly. This study converted relative humidity to water vapor pressure using relative humidity and saturated water vapor pressure. We calculated saturated water vapor pressure using the Magnus equation with coefficients from Alduchov and Eskridge (1996) and temperature from the meteorological sensor. Then, we performed error propagation to calculate uncertainties of water vapor pressure for the meteorological sensor at the estimation epoch.

Regarding the formal errors of NWM, we obtained the uncertainties from Balidakis (2019). However, these numbers are
220   valid only for this experiment because the formal errors of NWM vary on location and time. Unfortunately, we cannot extract
formal errors from GPT3 as this information is not provided. Therefore, we determined formal empirical errors of GPT3 by
computing the differences w.r.t the meteorological sensor for each meteorological parameter. Then, the RMS of the differences
was extracted. We used these values as formal errors for GPT3. Therefore, these numbers are only valid for this experiment.

Table A1. The uncertainties of meteorological parameters from Global Pressure Temperature 3, ERA5 Numerical Weather Model, and the
meteorological sensor (Vaisala WXT530).

Parameters	Global Pressure Temperature 3	Numerical Weather Model	Meteorological sensor
Pressure (hPa)	10.8	1	0.5
Temperature (°C)	3.1	1	0.3
Relative Humidity (%)	x	x	3.0
Water Vapor Pressure (hPa)	1	1	0.3

Data availability. The data that support the findings of this study are available from the corresponding author upon reasonable request.

225   *Author contributions.* CK did most of the data analysis and writing of the manuscript. CK, RH, and MR participated in the design of the
experiment and helped to improve the manuscript. KB, BM, and HS contributed to discussion of the results and improving the manuscript.
All the authors read and approved the final manuscript.

Competing interests. The authors declare that they have no conflict of interest.

Acknowledgements. We would like to thank to Deutscher Akademischer Austauschdienst (DAAD) for financial support by granting schol-
230   arship to the main author under grant number 91650950. We also would like to thank Mr. Thomas Gerber for kindly helping us to set up the
experiment. KB acknowledges funding from DFG for the Collaborative Research Centre TerraQ under INST 187/818-1.

References

Current IGS Site Guidelines, https://kb.igs.org/hc/en-us/articles/202011433-Current-IGS-Site-Guidelines, 2019.

Alduchov, O. A. and Eskridge, R. E.: Improved Magnus form approximation of saturation vapor pressure, Journal of applied meteorology, 35, 601–609, 1996.

Altamimi, Z., Rebischung, P., Métivier, L., and Collilieux, X.: ITRF2014: A new release of the International Terrestrial Reference Frame modeling nonlinear station motions, Journal of Geophysical Research: Solid Earth, 121, 6109–6131, 2016.

Balidakis, K.: On the development and impact of propagation delay and geophysical loading on space geodetic technique data analysis, Doctoral thesis, Technische Universität Berlin, Berlin, https://doi.org/10.14279/depositonce-9125, http://dx.doi.org/10.14279/depositonce-9125, 2019.

Balidakis, K., Nilsson, T., Zus, F., Glaser, S., Heinkelmann, R., Deng, Z., and Schuh, H.: Estimating integrated water vapor trends from VLBI, GPS, and numerical weather models: Sensitivity to tropospheric parameterization, Journal of Geophysical Research: Atmospheres, 123, 6356–6372, 2018.

Bock, O., Willis, P., Lacarra, M., and Bosser, P.: An inter-comparison of zenith tropospheric delays derived from DORIS and GPS data, Advances in space research, 46, 1648–1660, 2010.

Böhm, J., Werl, B., and Schuh, H.: Troposphere mapping functions for GPS and VLBI from ECMWF operational analysis data, Journal of geophysical research, 111, 1–9, 2006.

Chen, G. and Herring, T.: Effects of atmospheric azimuthal asymmetry on the analysis of space geodetic data, Journal of Geophysical Research: Solid Earth, 102, 20 489–20 502, 1997.

Dousa, J. and Vaclavovic, P.: Real-time zenith tropospheric delays in support of numerical weather prediction applications, Advances in Space Research, 53, 1347–1358, 2014.

Glaser, S., König, R., Neumayer, K. H., Nilsson, T., Heinkelmann, R., Flechtner, F., and Schuh, H.: On the impact of local ties on the datum realization of global terrestrial reference frames, Journal of Geodesy, 93, 655–667, 2019.

Heinkelmann, R., Willis, P., Deng, Z., Dick, G., Nilsson, T., Soja, B., Zus, F., Wickert, J., and Schuh, H.: Multi-technique comparison of atmospheric parameters at the DORIS co-location sites during CONT14, Advances in Space Research, 58, 2758–2773, 2016.

Kitpracha, C., Balidakis, K., Heinkelmann, R., and Schuh, H.: Assessment on atmospheric parameters at co-location sites, in: EGU General Assembly Conference Abstracts, p. 6517, 2020.

Krügel, M., Thaller, D., Tesmer, V., Rothacher, M., Angermann, D., and Schmid, R.: Tropospheric parameters: combination studies based on homogeneous VLBI and GPS data, Journal of Geodesy, 81, 515–527, 2007.

Lagler, K., Schindelegger, M., Böhm, J., Krásná, H., and Nilsson, T.: GPT2: Empirical slant delay model for radio space geodetic techniques, Geophysical research letters, 40, 1069–1073, 2013.

Landskron, D. and Böhm, J.: VMF3/GPT3: refined discrete and empirical troposphere mapping functions, Journal of Geodesy, 92, 349–360, 2018.

Männel, B., Thaller, D., Rothacher, M., Böhm, J., Müller, J., Glaser, S., Dach, R., Biancale, R., Bloßfeld, M., Kehm, A., Pinzón, I. H., Hofmann, F., Andritsch, F., Coulot, D., and Pollet, A.: Recent Activities of the GGOS Standing Committee on Performance Simulations and Architectural Trade-Offs (PLATO), in: International Symposium on Advancing Geodesy in a Changing World, edited by Freymueller, J. T. and Sánchez, L., pp. 161–164, Springer International Publishing, Cham, 2019.

Männel, B., Brandt, A., Nischan, T., Brack, A., Sakic, P., and Bradke, M.: GFZ final product series for the International GNSS Service (IGS), 2020.

270 Nilsson, T., Böhm, J., Wijaya, D. D., Tresch, A., Nafisi, V., and Schuh, H.: Path Delays in the Neutral Atmosphere, pp. 73–136, Springer Berlin Heidelberg, Berlin, Heidelberg, https://doi.org/10.1007/978-3-642-36932-2_3, 2013.

Petit, G. and Luzum, B.: IERS conventions (2010), Tech. rep., Bureau International des Poids et mesures sevres (France), 2010.

Pinzón, I. H. and Rothacher, M.: Assessment of local GNSS baselines at co-location sites, Journal of Geodesy, 92, 1079–1095, 2018.

Plag, H.-P., Rothacher, M., Pearlman, M., Neilan, R., and Ma, C.: The global geodetic observing system, in: Advances in Geosciences:

275 Volume 13: Solid Earth (SE), pp. 105–127, World Scientific, 2009.

Pollet, A., Coulot, D., Bock, O., and Nahmani, S.: Comparison of individual and combined zenith tropospheric delay estimations during CONT08 campaign, Journal of Geodesy, 88, 1095–1112, 2014.

Ray, J. and Altamimi, Z.: Evaluation of co-location ties relating the VLBI and GPS reference frames, Journal of geodesy, 79, 189–195, 2005.

Rebischung, P. and Schmid, R.: IGS14/igs14. atx: a new framework for the IGS products, in: AGU Fall Meeting 2016, 2016.

280 Schmid, R.: Zur Kombination von VLBI und GNSS, DGK, Reihe C, Heft 636, Verlag der Bayerischen Akademie der Wissenschaften, ISBN 978-3-7696-5048-8, 2009.

Schuh, H. and Böhm, J.: Very long baseline interferometry for geodesy and astrometry, in: Sciences of Geodesy-II, pp. 339–376, Springer, 2013.

Steigenberger, P., Hugentobler, U., Schmid, R., Hessels, U., Klügel, T., and Seitz, M.: GPS-specific local effects at the Geodetic Observatory

285 Wettzell, in: Reference frames for applications in geosciences, pp. 125–130, Springer, 2013.

Teke, K., Böhm, J., Nilsson, T., Schuh, H., Steigenberger, P., Dach, R., Heinkelmann, R., Willis, P., Haas, R., García-Espada, S., et al.: Multi-technique comparison of troposphere zenith delays and gradients during CONT08, Journal of Geodesy, 85, 395, 2011.

Teke, K., Nilsson, T., Böhm, J., Hobiger, T., Steigenberger, P., García-Espada, S., Haas, R., and Willis, P.: Troposphere delays from space geodetic techniques, water vapor radiometers, and numerical weather models over a series of continuous VLBI campaigns, Journal of

290 Geodesy, 87, 981–1001, 2013.

Uhlemann, M., Gendt, G., Ramatschi, M., and Deng, Z.: GFZ global multi-GNSS network and data processing results, in: IAG 150 years, pp. 673–679, Springer, 2015.